Engineering Models for Plastic Fracture Analysis of Cylindrical Pressure Vessels and Piping

A. Ranta-Maunus
Department of Reactor Safety, Institute of Radiation Protection, P.O. Box 268, SF-00101 Helsinki 10, Finland

Cylinders with long axial and circumferential surface flaws are analyzed under pressure, thermal gradient and external force. Fully plastic material behaviour is adopted at the cracked cross-section, and linear elastic response for the rest of the cylinder. Analytical expressions have been derived for CTOD and T-modulus as a function of loads, crack size, flow stress and dimensions.

The results which are applicable to large scale yielding in the cracked cross-section indicate that the size of the pressure vessel, radius, is an important variable affecting CTOD. In the case of axial flaws in cylinders with the same wall thickness but different radius (and different design pressure), CTOD is linearly dependent upon the radius. The expressions for T-modulus show a dependence on the radius-to-wall thickness ratio.

Numerical results are illustrated in two cases which are typical of a BWR pressure vessel and PWR primary circuit piping. In the latter case, the combination of ductile material and small radius of cylinder makes the initiation of stable crack growth very unlikely under any loading less than the plastic limit load of the flawed cylinder. Accordingly, the analysis suggests that the simple net-section stress method is appropriate for the analysis of flawed ductile piping. The same conclusion must not be made for larger cylinders for which the net-section stress method is unconservative.

The values of T-modulus are mainly dependent on the value of pressure in the case of axial flaws. For solely thermal loading in the presence of axial flaws as well as for both axial and thermal loads in the presence of circumferential flaws we obtain small values of T-modulus, below 50 in all cases.

1. Introduction

This paper summarizes a work made to develop simple analytical expressions for the fracture analysis of ductile cylindrical pressure vessels and piping. The work is restricted to ideal flaw shapes. Equideep longitudinal and circumferential surface flaws inside the cylinder are analyzed under pressure and thermal loads.

The material behaviour is assumed to be linear elastic outside the cracked cross-section, and displacements are calculated by conventional strength-of-materials methods. The direct effect of pressure on crack faces is neglected. The material in the cracked ligament is presumed to be ideally plastic. Crack tip opening displacement has been adopted as the criteria of crack initiation and growth. Analytical expressions have been derived for CTOD and tearing modulus T.

2. Description of method

The analysis of a long axial flaw on the inside of a cylinder has been reported in detail in an earlier paper /1/. A similar but more simplified analysis of a circumferential flaw around the cylinder will be introduced in the following.

The cylinder is assumed to be cut into two pieces through the cracked plane (Fig 1.). The fully yielded ligament transmits a bending moment denoted by M_y. The loadings are a remote axial stress, σ_{ax}, which can be caused by internal pressure or external force, and a thermal gradient through the wall which is constant everywhere in the cylinder and results in a bending stress, σ_T, presumed to be linear for simplicity. The rotation of the cracked cross-section is illustrated in Fig. 2, as well as the stress distribution in the ligament. Note that different values can be adopted as axial flow stress in tension and compression.

In accordance with strenght-of-materials textbooks, we obtain for the rotation of the end of a thin-walled cylinder loaded by bending moment

$$\phi = 8.5 \frac{M}{Et^2} \sqrt{\frac{R}{t}} \qquad (1)$$

The bending moment consists of two parts, $M = M_y + M_T$, of which M_y can be easily integrated from the stress distribution shown in Fig. 2, and M_T is the bending moment induced by thermal stresses, $M_T = \sigma_T t^2/6$. In this point, ϕ given by eq. (1) is dependent on the location of the rotation axis, b, which can be solved from the axial force equilibrium equation. By the adoption of $\sigma_y = \sigma_o$ we obtain

$$\frac{b}{t} = \frac{1}{2}\left(1 - \frac{a}{t} + \frac{\sigma_{ax}}{\sigma_y}\right) \qquad (2)$$

Finally, the bending moment M in eq. (1) being known, the crack tip opening displacement can be calculated as follows

$$\delta = 2b\phi = 17 \frac{M}{Et^2} \frac{b}{t} \sqrt{Rt} \tag{3}$$

When the values of J-integral and tearing modulus are of interest, the following relations have been applied

$$J = m \sigma_y \delta \tag{4}$$

$$T = \frac{mE}{\sigma_y} \frac{d\delta}{da} \tag{5}$$

with m = 1.

3. Axial flaw in cylinder

3.1 Analytical expressions

The behaviour of a cylinder with a long axial flaw at the inner surface is analyzed under pressure and thermal loads. As shown in /1/, an analytical expression can be obtained for CTOD δ and tearing modulus T. For the case with $\sigma_y / \sigma_o = 2$ in Fig. 2 we rewrite the expressions as follows

$$\delta = 2\pi R \frac{1-\nu^2}{E} \sigma_y \left(1 - \frac{a}{t} + 2 \frac{\sigma_m}{\sigma_y}\right) C \tag{6}$$

$$T = 2\pi \frac{R}{t} (1 - \nu^2) \left[\frac{4}{9} \left(1 - \frac{a}{t} + 2 \frac{\sigma_m}{\sigma_y}\right)^2 - C\right] \tag{7}$$

where

$$C = \frac{2}{9} \left[\frac{\sigma_T}{\sigma_y} + \frac{\sigma_m}{\sigma_y}\left(2 \frac{\sigma_m}{\sigma_y} + 4 \frac{a}{t} - 1\right) - \left(1 - \frac{a}{t}\right)^2\right] \tag{8}$$

$$\sigma_T = 6 M_T / t^2 \ , \ \sigma_m = pR/t$$

Thus σ_T is the linearized thermal stress induced by different inside and outside temperatures. The positive sign of σ_T refers to tension at the inner surface.

Eq. (6) shows clearly that CTOD, which is a characteristic of crack growth initiation, is linearly dependent upon the radius of the cylinder. On the other hand, the criterion of instability, T-modulus, appears to depend linearly on the relation R/t as shown in eq. (7). The conclusion is simply that cracks in large-diameter and relatively thinwalled cylinders are more likely to cause severe failures than those in smaller or thick-walled cylinders when the material obeys ductile behaviour.

3.2 Application to pressure vessel

Eqs. (6) and (7) are applied to two numerical examples summarized in Table 1. Example 1 is typical of a BWR pressure vessel made of A533B steel. Fig. 3 illustrates the results as equal value curves of CTOD in a coordinate system of load vs. crack size. Fig. 4 shows a stability assessment diagram with reference to material resistance values taken from literature /2/.

The curves in Fig. 3a terminate at points where the plastic limit load is reached (c = 0 in Fig. 2). In Figs. 3b and 3c the curves are terminated at points where the overall mechanical behaviour of the cylinder is no longer considered to be linear elastic. The results show that for flaws a/t < 0.3, the design pressure does not make the cracked cross-section fully yielded, and accordingly the crack is practically closed. The thermal moment alone resulting in $\sigma_T = 2\ S_m$ (S_m refers to the allowable membrane stress in ASME Code) can cause crack initiation if the critical value of CTOD is not more than 1 mm, but no unstable growth. The third case illustrated is the combination of thermal gradient with design pressure (Fig. 3c). In accordance with ASME Code, the allowable value of thermal stress is here roughly $\sigma_T = 2\ S_m$. For this loading, the crack height causing a fully plastic ligament appears to be less than 10 % of the wall thickness.

The instability assessment of cracks is illustrated in Fig. 4. First of all we notice that the curves are quite different from those in EPRI Fracture Handbook /2, Fig. 7-4/. In this study with ideally plastic material, the applied CTOD-T curves do not start from the origin. Secondly, the plastic limit load is reached before tearing instability in the case of a/t = 0.75 (not shown in Fig. 4). Two reasons for the discrepancies are obvious: EPRI applies a strain hardening material model and the ratio R/t = 10. The applied CTOD-T curve is also illustrated in the case of design pressure combined with increasing thermal stress as well as in the case of pure thermal loading, both for a/t = 0.25. The curves indicate the important role of pressure as a reason for crack instability.

3.3 Application to piping

In the case of stainless steel piping (Example 2), no stability assessment diagram is shown simply because all the cases of loading are very far from unstable growth: applied $T \leq 70$, applied CTOD ≤ 1 mm. Furthermore, the initation of stable growth in stainless steel is not expected for any loading combination for which the overall response of the cylinder remains elastic. Accordingly, we conclude that the net-section stress method is appropriate for the analysis of axial flaws in ductile piping. The results of Example 2 are illustrated in Fig. 5. The curves for pressure load in Fig. 5a terminate at points corresponding to the plastic limit load. The termination of curves in Figs. 5b and 5c indicates the initiation of the second plastic hinge in the cylinder.

4. Circumferential flaw in cylinder

The cylindrical pressure vessel or pipe is analyzed also in the case of a circumferential flaw around the cylinder. The application of eqs. (2), (3) and (5) reveals

$$\delta = 2.12 \sqrt{Rt}\, \frac{\sigma_y}{E} \left(1 - \frac{a}{t} + \frac{\sigma_{ax}}{\sigma_y}\right) C \qquad (9)$$

$$T = 2.12 \sqrt{\frac{R}{t}} \left[2\left(1 - \frac{a}{t} + \frac{\sigma_{ax}}{\sigma_y}\right)^2 - C\right] \qquad (10)$$

where

$$C = \frac{2\sigma_T}{3\sigma_y} + \left(\frac{\sigma_{ax}}{\sigma_y}\right)^2 + 2\,\frac{\sigma_{ax}}{\sigma_y}\,\frac{a}{t} - \left(1 - \frac{a}{t}\right)^2 \qquad (11)$$

Here CTOD is linearly dependent on factor $\sqrt{Rt}$ and tearing modulus is proportional to $\sqrt{R/t}$.

Numerical results are calculated for Example 1 in Table 1 (BWR RPV) when loaded by the combination of design pressure and thermal stress. Results in Fig. 6 illustrate that CTOD does not exceed 1 mm in the case of circumferential cracks with $a < 0.7\ t$, and when allowable stresses are not exceeded. Under this loading, the value of T is below 20.

Results for Example 2 piping loaded by the simultaneous application of axial force and the constant thermal stress $\sigma_T = 2S_m$ are shown in Fig. 7. We notice that the line CTOD = 0.5 mm is close to the plastic limit load line $c = 0$. Accordingly, the net-section stress method is applicable to materials tolerating CTOD = 0.5 mm. The maximum value of applied T-modulus is $T = 38$ and it is obtained in a hypothetical case where $\sigma_{ax} = \sigma_y$ and $a = 0$.

5. Discussion

The results shown in this paper are greatly influenced by the selection of flow stress values σ_y and σ_o (Fig. 2). The purpose in selecting them was to simulate real strain hardening materials as well as possible, i.e. the bending moments transmitted by the cracked cross-section should be the same. The selection $\sigma_y = 2\,\sigma_o$ for axial flaw, when σ_y is the mean value of engineering yield and ultimate stresses in uniaxial tensile test, has been verified by a FEM calculation /3/.

Axial and circumferential flaws in cylinders have also been analyzed by the application of the slip-line method. Expressions of CTOD are of a similar form, as will be reported by Mr. Keskinen in this conference /4/.

The results illustrated in Figs. 3 and 5 have been compared to those given by LEFM with plastic zone correction. SIF for axial flaws is calculated

$$K_I = \left(\frac{2p\,R_o^2\,F}{R_o^2 - R^2} + \sigma_T\,M_b\right)\sqrt{\pi(a + r_y)} \qquad (12)$$

where $r_y = \frac{1}{6\pi} \left(\frac{K_I}{\sigma_y}\right)^2$

The influence of pressure on K_I has been adopted from EPRI Fracture Handbook /3, eq. (4-1)/ including notations, and M_b has been taken from ASME Code. The relation between δ and K_I has been calculated as

$$\delta = \frac{1 - \nu^2}{E\,\sigma_y} K_I^2 \qquad (13)$$

In general, the application of eqs. (12) and (13) gives results comparable to the fully plastic analysis in the range of CTOD = 0.2 mm (corresponding to K_I = 110 - 140 MPa $\sqrt{m}$) in Figs. 3 and 5. When CTOD is greater, LEFM becomes rapidly inapplicable because also r_y is increasing, approximatively r_y = 30 CTOD. This comparison suggests roughly that CTOD = 0.2 mm could act as a borderline between the application of elastic and plastic analyses.

6. Conclusions

The results show that ductile pressure vessels tolerate large flaws before failure. The main conclusion is that the assurance of ductility and high toughness of materials is of primary importance.

The results for axial flaws indicate that the size of cylinder, radius, is one of the most important variables having influence on the crack initiation. This suggests that for small diameter cylinders with ductile materials, such as piping, the application of the net-section stress method is appropriate. For larger diameter cylinders it is unconservative and a more advanced analysis is needed. Because the flaws in large cylinders are more likely to grow, the NDE requirements should be dependent on the size of the pressure vessel.

In the presence of circumferential flaws, the important size parameter characteristic of crack initiation is $\sqrt{Rt}$. The numerical results confirm, as has been known earlier, that circumferential flaws in ductile cylinders are very unlikely to experience stable growth under practical loads.

References

/1/ Ranta-Maunus A.K., Achenbach J.D., "A simple model for stability of a long axial surface crack in a thin walled cylinder", Int. J. Mech. Sci 24, 313-321 (1982).

/2/ Kumar V., German M.D., Shih C.F., "An engineering approach for elastic-plastic fracture analysis", EPRI NP-1931 (July 1981).

/3/ Ranta-Maunus Alpo, Talja Heli, "Elasto-plastic analysis of a cracked ductile cylindrical pressure vessel", Int. J. Pressure Vessels and Piping (to be published).

/4/ Keskinen R.P., "Elastoplastic analysis of surface cracks in pressure vessels using slip-line field theory", SMiRT 7 G/F 3/2.

Table 1. Numerical values used in examples.

Example	t [mm]	R [mm]	σ_y [MPa]	E [MPa]	ν	p_{des} [MPa]	S_m [MPa]
1	134	2770	420	$2.1 \cdot 10^5$	0.3	8.5	175
2	61	350	310	$1.8 \cdot 10^5$	0.3	17	117

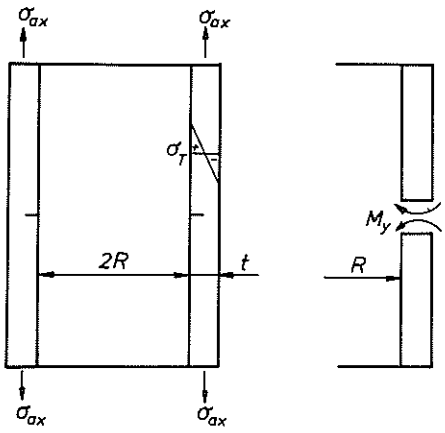

Fig. 1 Cylinder with a circumferential flaw loaded by remote axial stress σ_{ax} and linearized thermal stress σ_T.

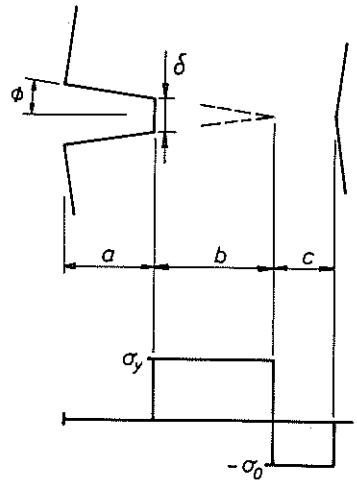

Fig. 2 Rotation in the cracked cross-section, and a fully plastic stress distribution.

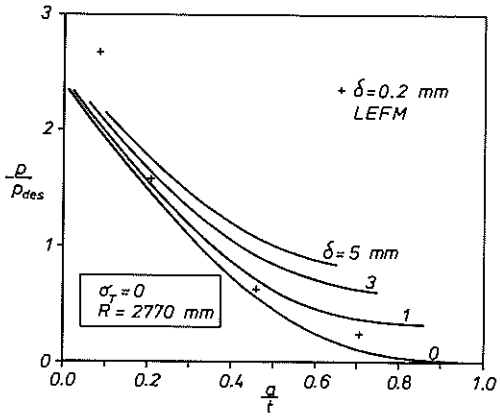

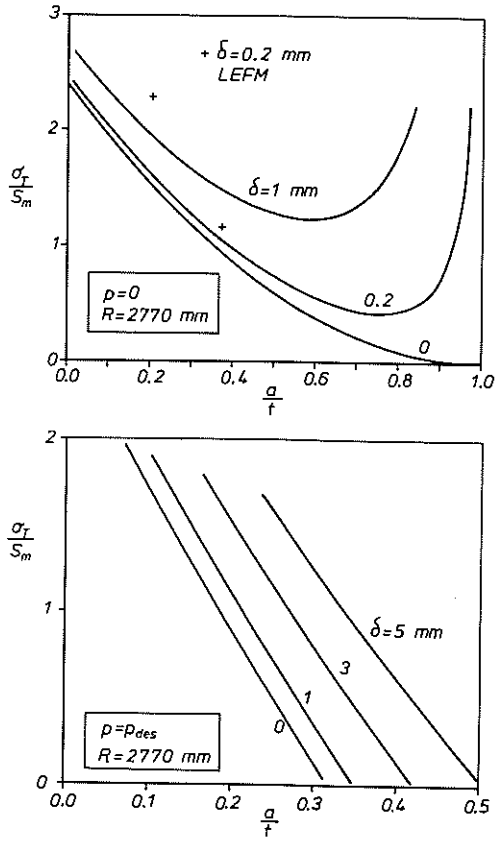

Fig. 3 Equal value curves of CTOD in Example 1 characterizing a BWR pressure vessel with an axial flaw. (a) Pressure load only, (b) thermal load only, and (c) design pressure p_{des} combined with variable thermal stress. The points for "LEFM" refer to eqs. (12) and (13).

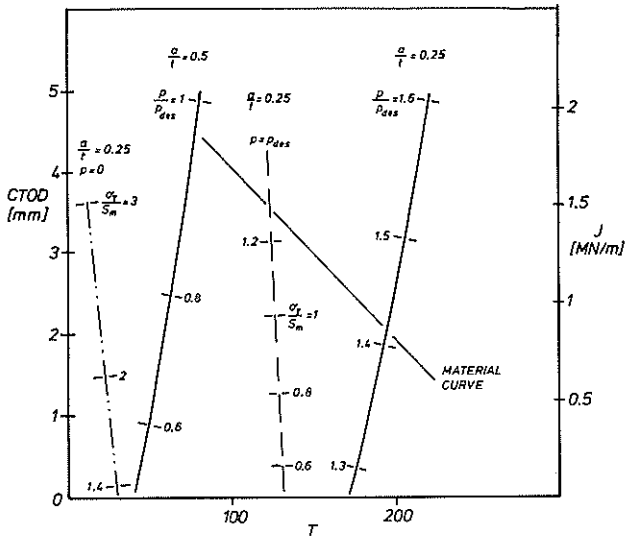

Fig. 4 Stability assessment diagrams for Example 1. Material curve refers to A 533B /2/.

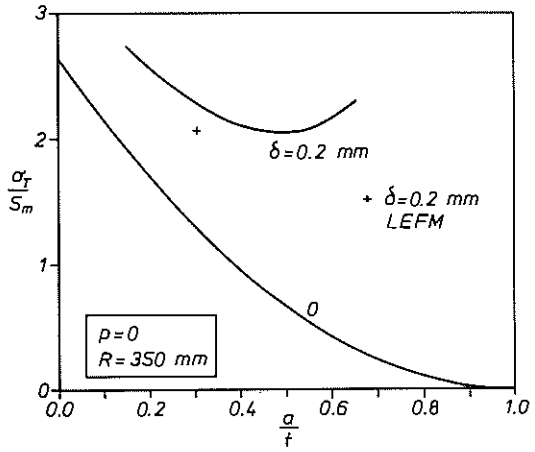

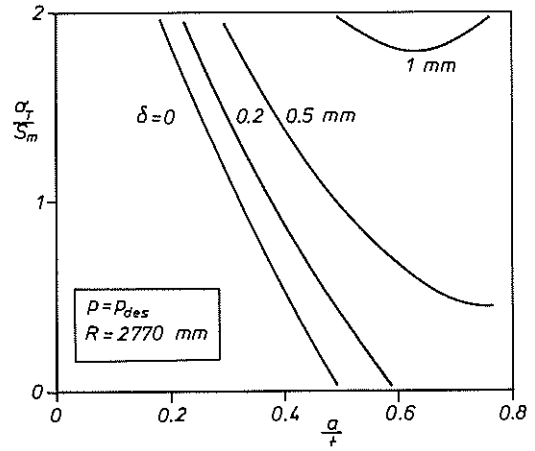

Fig. 6 Equal value curves of CTOD in Example 1 with a circumferential flaw under the combined loading of design pressure and thermal gradient.

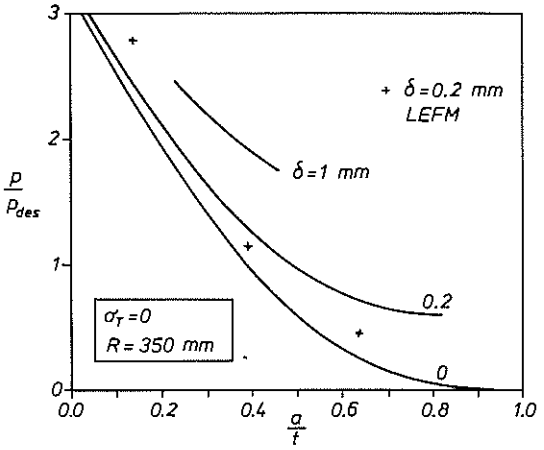

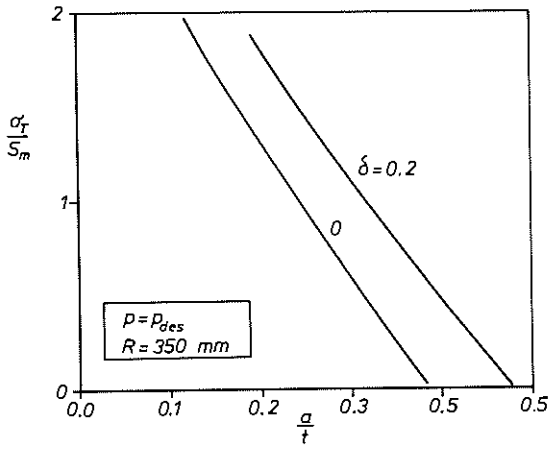

Fig. 5 Equal value curves of CTOD in Example 2 characterizing stainless steel piping with an axial flaw. (a) Pressure load only, (b) thermal load only, and (c) design pressure combined with variable thermal stress. The points of "LEFM" refer to eqs. (12) and (13).

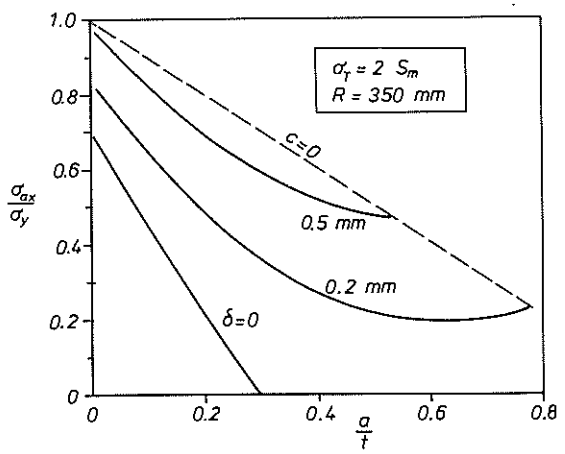

Fig. 7 Equal value curves of CTOD in Example 2 with a circumferential flaw under the combined loading of thermal stress $\sigma_T = 2\ S_m$ and tensile force.